

# MODELING IMPACT OF GRAVITY WAVES ON THE THERMOSPHERE OF MARS WITH A NON-OROGRAPHIC WHOLE ATMOSPHERE GRAVITY WAVE SCHEME: M-GITM APPLICATION FOR INTERPRETING MAVEN MEASUREMENTS

S. W. Bougher, K. J. Roeten, *CLASP Department, U. of Michigan, Ann Arbor, MI, USA, ([bougher@umich.edu](mailto:bougher@umich.edu))*, E. Yiğit, Department of Physics and Astronomy, George Mason University, Fairfax, VA USA, A. S. Medvedev, Max Planck Institute., Germany, M. K. Elrod, M. Benna, NASA Goddard Space Flight Center, Greenbelt, MD USA.

## Introduction:

Gravity waves are ubiquitous throughout the Mars atmosphere. They play an important role in producing the general circulation pattern and temperature structure in the middle and upper atmosphere of Mars (e.g., Medvedev and Yiğit, 2012) and facilitate cloud formation in the upper mesosphere and lower thermosphere (Yiğit et al., 2018). Expected variations of this thermosphere structure and winds owing to changing solar insolation are significantly modified by upward propagating gravity waves. Indeed, the effects of GWs in the Martian upper atmosphere have been observed by the MAVEN (Mars Atmosphere Volatile Evolution) mission up to at least 250 km (Yiğit et al. 2015). Nevertheless, a comprehensive characterization of GWs in the Martian upper atmosphere is still lacking. In this regard, improvements in numerical modeling can serve to address the impacts of GWs on the upper atmosphere. For this, we implement a state-of-the-art GW scheme into a Martian General Circulation Model and study GW effects in the thermosphere. We provide a possible interpretation of the thermospheric temperatures retrieved from MAVEN.

MAVEN Neutral Gas and Ion Mass Spectrometer (NGIMS) measurements include both Science Orbits (SO) and a set of 9-Deep Dip (DD) campaign orbits throughout the mission. Neutral argon densities are typically used to extract corresponding thermospheric temperatures. SO sampling and temperature extraction typically occurs above ~150 km, while DD campaign sampling can reach to ~125 km, providing lower thermospheric measurements. For the latter, Deep Dip 2 (DD2) near noon at the equator is selected for detailed study of its extracted temperature profile (Stone et al. 2018). General circulation model (GCM) simulations to date (using modern EUV heating efficiencies, but without accounting for

subgrid-scale GWs) have found it difficult to reproduce the details of this DD2 profile. Similarly, recent NGIMS measurements of global thermospheric wind components can be interpreted using general circulation models (Benna et al., 2019; Roeten et al. 2019). GCM simulations with solar forcing alone cannot capture the full range of variability or the campaign averaged behavior seen in these measured winds over roughly 10-orbit monthly campaigns spanning ~150-220 km. This missing GW physics is likely an important underlying factor.

## M-GITM Model and GW Scheme Setup:

To examine the thermospheric impacts of using a modern GW scheme, new Mars Global Ionosphere-Thermosphere Model (M-GITM) (Bougher et al. 2015) simulations are conducted and outputs compared to corresponding DD2 temperatures and global winds from selected NGIMS campaigns. Modern M-GITM model simulations are driven by daily solar EUV-UV fluxes (from the MAVEN/EUVM instrument). Specifically, EUVM daily fluxes from the FISM-M empirical model (Thiemann et al., 2017) are used to supply inputs to the M-GITM code for calculating solar EUV-UV heating, photo-dissociation, and photo-ionization rates (e.g., Roeten et al. 2019). In addition, a fast and modern formulation for non-LTE CO<sub>2</sub> 15- $\mu$ m cooling is now used within the M-GITM code from Gonzalez-Galindo et al. (2013). This scheme serves to accurately capture the CO<sub>2</sub> cooling rates, especially near the mesopause.

Most importantly, a spectral nonlinear whole atmosphere GW scheme (Yiğit et al. 2008, Medvedev and Yiğit, 2012) is newly incorporated into M-GITM, using a robust set of standard GW parameters, and its impact on thermospheric temperatures and winds is investigated. Specifically, the global distribution of gravity wave momentum and energy deposition terms are now computed interactively for the M-GITM

code (Roeten et al., 2022). This GW scheme is tailored for the treatment of non-orographic gravity waves that reach the thermosphere from their launching point at the top of the planetary boundary layer. This scheme is one of the most recent parameterizations appropriate for gravity waves that propagate to thermospheric altitudes. It accounts for wave dissipation due to molecular viscosity in the upper atmosphere, molecular thermal conduction, radiative damping, and nonlinear breaking-saturation (Yigit et al., 2008). Standard gravity model parameters utilized in M-GITM code are as follows: (a) horizontal wavelength (300 km), (b) GW spectrum source height (~top of the planetary boundary layer, ~9 km), and (c) the momentum source flux ( $0.0025 \text{ m}^2/\text{s}^2$ ). Some of these key parameters are based upon existing GW measurements obtained by MAVEN and previous Mars missions, e.g. horizontal wavelength (Medvedev et al. 2011); other parameters are unconstrained thusfar (e.g. momentum source flux).

### General Modeling Results:

For initial investigation, we have selected  $L_s \sim 270\text{-}280^\circ$  seasonal conditions (only), and solar moderate EUV-UV fluxes. Key fields (temperatures plus zonal and meridional winds) are compared with and without GW effects included. These fields are specifically plotted for zonally and temporally ( $15^\circ \Delta L_s$ ) averaged values, for ease of comparison with previous MGCM simulations incorporating the whole atmosphere GW scheme (e.g., Medvedev et al., 2011; Yigit et al., 2018).

Figures 1 and 2 illustrate that the chosen spectrum of GWs primarily deposits its momentum and energy over a range of altitudes from ~90-160 km.

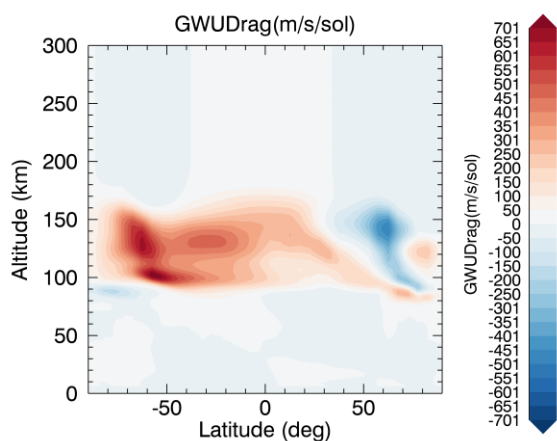


Figure 1: Zonal momentum deposition rate in units of m/s/sol. 15-day zonal average.

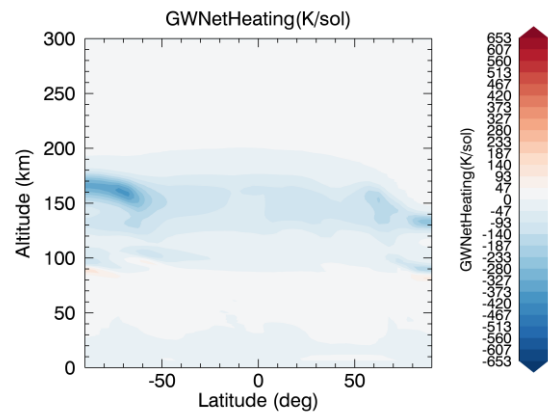


Figure 2: Zonal energy deposition rate in units of K/sol. 15-day zonal average.

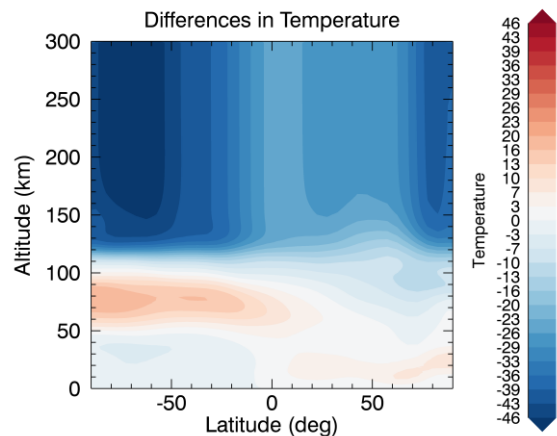


Figure 3. Temperature differences for two cases: GW case temperatures minus no GW case values (K).

The net impacts on simulated M-GITM temperatures (see Figure 3) are twofold: (a) significant cooling in the thermosphere at all latitudes, but especially at high-latitudes (up to  $45^\circ\text{K}$  cooling at S. polar region), and (b) S. hemisphere warming (up to  $\sim 20 \text{ K}$ ) at mesosphere altitudes ( $\sim 60\text{-}90 \text{ km}$ ). The latter can be compared with the MRO/MCS temperature climatology up to about  $\sim 90 \text{ km}$ .

The corresponding net impacts on zonal and meridional winds are best represented by raw wind plots, for which “no GW” and “with GW” case wind components are compared visually (see Figure 4). Generally, zonal wind magnitudes are reduced by

about a factor of  $\sim 2$  with the incorporation of the GW momentum term. In addition, the single westerly “deep” zonal jet (spanning 0-250 km, in the summer hemisphere ) is now nearly closed off over  $\sim 100$ -130 km altitude, giving rise to separate westerly jets in the lower atmosphere (peaking at  $\sim 50 \pm 25$  km) and in the thermosphere (above  $\sim 150$  km).

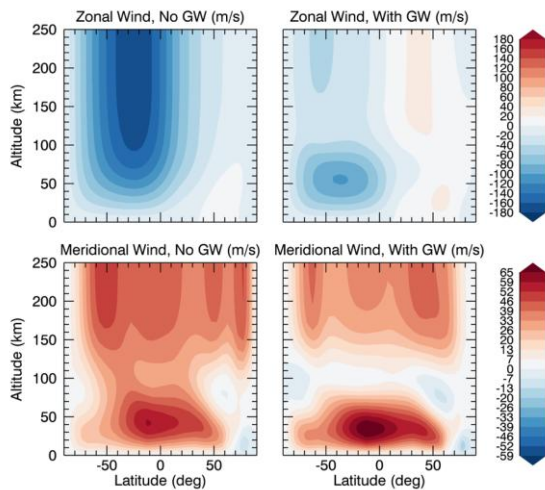


Figure 4: Zonal and meridional wind plots for: (a) left column (“no GW” case), and (b) right column (“with GW” case). Wind magnitudes are in units m/s.

### Specific Modeling Results: Data Comparisons

Specific simulations using M-GITM were conducted (with and without GWs) corresponding to the DD2 campaign in April 2015. This was the portion of the MAVEN mission when solar fluxes were near the peak of solar cycle #24 conditions. Corresponding seasonal conditions were near  $L_s \sim 328$  (after perihelion). Finally, extracted NGIMS DD2 temperatures sampled at low SZA ( $\sim 9.0^\circ$ ) are compared to newly simulated M-GITM profiles.

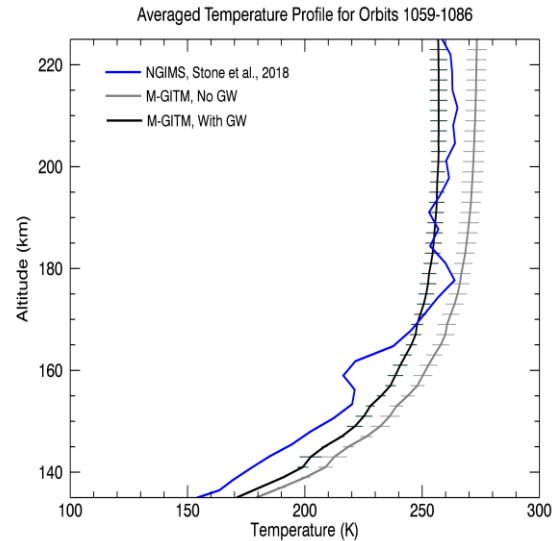


Figure 5: DD2 campaign averaged temperature profiles: (a) NGIMS derived (from Stone et al. 2018), (b) M-GITM “no GW” case, and (c) M-GITM “with GW” case. Simulated cross-hatched lines corresponds to the  $1\text{-}\sigma$  variability of the orbit-orbit temperatures around the computed mean.

Figure 5 shows the simulated temperature profile including GWs is cooler by  $\sim 15\text{-}20^\circ\text{K}$  (above 180 km) and  $\sim 10\text{-}15^\circ\text{K}$  at lower altitudes. These computed temperatures are much closer to NGIMS extracted values. The reason for this improvement is due to the slowed circulation, which reduces the transport of atomic O from the dayside to the nightside of Mars. This yields increased dayside O/CO<sub>2</sub> ratios near  $\sim 150$  km where the CO<sub>2</sub> 15- $\mu\text{m}$  cooling layer peaks. These O abundances now match NGIMS measured values in the lower thermosphere. Recall that collision of O and CO<sub>2</sub> enhances 15- $\mu\text{m}$  emission under non-LTE conditions (e.g. Bougher et al. 2017). Direct cooling of the thermosphere by GWs has also been modeled on Earth using the whole atmosphere scheme (Yigit and Medvedev, 2009), suggesting that GWs should be included in the energy balance of the thermosphere.

New M-GITM simulations were also run for the January 2017 NGIMS neutral wind observational campaign. Figure 6 shows both the averaged NGIMS velocities and corresponding M-GITM simulations, with and without GWs. This campaign occurred over Jan 11-13, 2017, from  $L_s=297\text{-}299$  (in the southern summer season), near midnight local time, and over southern mid-latitudes.

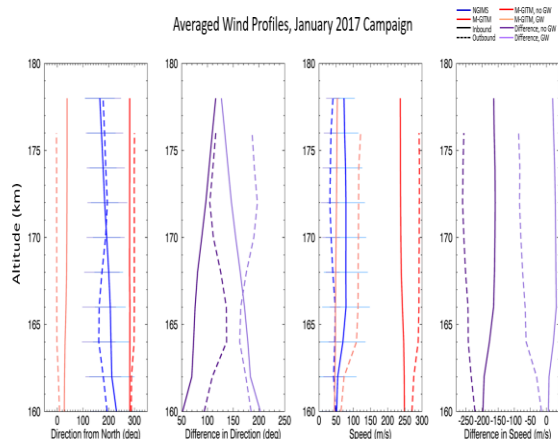


Figure 6. Data-model comparison plots for the January 2017 wind campaign illustrate the improvement of the computed mean wind magnitude, but no improvement in the direction with the “with GW” case.

With the addition of the GW scheme, the M-GITM wind speed profile slows by over 100 m/s, bringing it much closer to the averaged values observed by NGIMS. The simulated direction also shifts with the addition of GW effects, becoming less easterly and more westerly, while retaining the southerly component. While it cannot be said that this aspect of the data-model comparison improves, comparing the mean direction is difficult in this particular campaign due to extreme orbit-to-orbit variability in wind direction observed by NGIMS at the time.

Overall, these upgraded M-GITM simulations demonstrate that gravity waves can have a significant influence in shaping thermospheric winds and temperatures at low and high latitudes.

#### References:

Benna, M., S. Bougher, Y. Lee, K. Roeten, E. Yiğit, P. Mahaffy, B. Jakosky (2019), *Science*, doi:10.1126/science.aax1553

Bougher, S.W., Pawlowski, D., Bell, J. M., Nelli, S. McDunn, T., Murphy, J. R., et al. (2015). *JGR: Planets*, 120. doi.org/10.1002/2014JE004715

Bougher, S. W., D. A. Brain, J. L. Fox, F. Gonzalez-Galindo, C. Simon-Wedlund, and P. G. Withers (2017). Chapter 14 in *The Atmosphere and Climate of Mars*, ed. B. Haberle, M. Smith, T. Clancy, F. Forget, R. Zurek, Cambridge University Press, doi:10.1017/9781107016187.

González-Galindo, F., Chaufray, J.-Y., López-Valverde, M., Gilli, G., Forget, F., et al. (2013). *JGR: Planets*, 118. doi.org/10.1002/jgre.20150

Medvedev, A. S., Yiğit, E., Hartogh, P., & Becker, E. (2011). *JGR*, 116, doi: 10.1029/2011JE003848

Medvedev, A. S., and Yiğit, E. (2012), *GRL*, 39, L05201, doi:10.1029/2012GL050852.

Roeten, K J., S. W. Bougher, M. Benna, P. R. Mahaffy, Y. Lee, D. Pawlowski, F. Gonzalez - Galindo, M. A. Lopez-Valverde (2019), *JGR*, 124, 1-21. doi:10.1029/2019JE005957

Roeten, K.J., Bougher, S. W., Yiğit, E., Medvedev, A. S., Benna, M. and Elrod, M. K., (2022). Impacts of Gravity Waves in the Martian Thermosphere using M-GITM Coupled with a Whole Atmosphere Gravity Wave Scheme. *JGR: Planets*, submitted.

Stone, S.W., Yelle, R. V., Benna, M., Elrod, M. K., & Mahaffy, P. R. (2018). *JGR*, 123, 2842–2867. doi.org/10.1029/2018JE005559

Thiemann, E. M. B., Chamberlin, P. C., Eparvier, F. G., Templeman, B., Woods, T. N., Bougher, S.W., & Jakosky, B.M. (2017). *JGR: Space Physics*, 122, 2748–2767. doi.org/10.1002/2016JA023512

Yiğit and Medvedev (2009), *GRL*, 36, doi :10.1029/2009GL038507.

Yiğit, E., A. D. Aylward, and A. S. Medvedev (2008), *JGR*, 113, doi:10.1029/2008JD010135

Yiğit, E., S. L. England, G. Liu, A. S. Medvedev, P. R. Mahaffy, T. Kuroda, B. M. Jakosky (2015), *GRL*, 42, doi:10.1002/2015GL065307.

Yiğit, E., A. S. Medvedev, P. Hartogh, (2018), *Ann. Geophys.*, 36, 1631-1646, doi: 10.5194/angeo-36-1631-2018.